

## Circularly Polarized Light Can Override and Amplify Asymmetry in Supramolecular Helices

Jun Su Kang, Sungwoo Kang, Jong-Min Suh, Soon Mo Park, Dong Ki Yoon, Mi Hee Lim, Woo Youn Kim, and Myungeun Seo\*

Cite This: *J. Am. Chem. Soc.* 2022, 144, 2657–2666

Read Online

ACCESS |



Metrics &amp; More

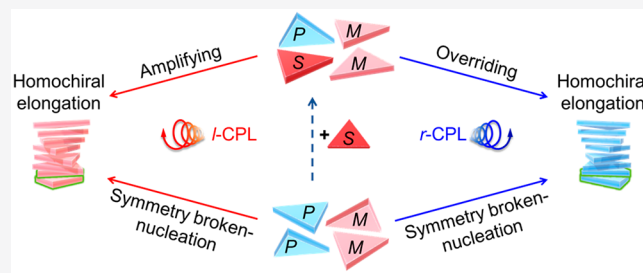


Article Recommendations



Supporting Information

**ABSTRACT:** Circularly polarized light (CPL) is an inherently chiral entity and is considered one of the possible deterministic signals that led to the evolution of homochirality. While accumulating examples indicate that chirality beyond the molecular level can be induced by CPL, not much is yet known about circumstances where the spin angular momentum of light competes with existing molecular chiral information during the chirality induction and amplification processes. Here we present a light-triggered supramolecular polymerization system where chiral information can both be transmitted and nonlinearly amplified in a “sergeants-and-soldiers” manner. While matching handedness with CPL resulted in further amplification, we determined that opposite handedness could override molecular information at the supramolecular level when the enantiomeric excess was low. The presence of a critical chiral bias suggests a bifurcation point in the homochirality evolution under random external chiral perturbation. Our results also highlight opportunities for the orthogonal control of supramolecular chirality decoupled from molecular chirality preexisting in the system.



## INTRODUCTION

Life on earth evolved to exclusively use one form of enantiomeric molecule out of a mirror-image pair. This prevailing single chirality implies that an event of symmetry breaking occurred in the racemic mixture at an early stage of life.<sup>1,2</sup> Circularly polarized light (CPL) from the universe has been proposed as one possible deterministic source of the asymmetry behind the chiral bias.<sup>3,4</sup> Because there are slightly different molar extinction coefficients for right-handed (*r*) and left-handed (*l*) CPL, defined as an anisotropy factor, one isomer preferentially undergoes a photochemical reaction upon CPL irradiation to create an enantiomeric excess (e.e.).<sup>5,6</sup> The CPL-induced photolysis of racemic amino acids has been shown to generate e.e. values of up to 4%.<sup>7,8</sup> Autocatalytic<sup>9</sup> or crystallization<sup>10</sup> processes have been suggested as possible chirality amplification pathways, which further increase e.e.

Transmission of chiral information from the enriched enantiomer to other molecules is also possible via a chirality induction process, which is key to the asymmetric organic synthesis and stereoregular polymerization.<sup>11</sup> Partial photo-resolution using CPL has been utilized to direct the helical organization of achiral media with a specific screw sense in liquid crystals<sup>12–15</sup> and polymers.<sup>16,17</sup> However, it is very unlikely that the chemical environments of the prebiotic stage would have been continuously exposed to CPL with a constant handedness. Random perturbation by an external chiral input would restore the system to the entropically favored racemic

state.<sup>18</sup> To realize an everlasting homochiral arrangement via chirality induction, molecular chirality needs to accumulate in competition with CPL to reach a critical e.e. that leads to bifurcation.<sup>2</sup> However, not much is known about how a system responds when both molecular and external chiral information are simultaneously transmitted.<sup>19</sup>

We hypothesized that it would be possible to examine the interplay of molecular chirality with external chiral input in supramolecular polymers. Helical self-assembly with a specific twist direction can occur depending on the configuration of the stereocenter in the monomer and amplify the chiral response.<sup>20</sup> Even when the transiently chiral building blocks lack permanent chirality, a one-handed helical conformation can prevail in a coassembly with a small number of permanently chiral inducers. This “sergeants and soldiers” (SaS) process is a good example of chirality induction, where the information from the “sergeant” is transmitted into the “soldiers” via noncovalent interaction (Figure 1a).<sup>21,22</sup> Recently, it was shown that it is possible to directly dictate the screw sense of supramolecular chirality by using CPL (Figure 1b).<sup>23–26</sup>

Received: October 26, 2021

Published: February 3, 2022



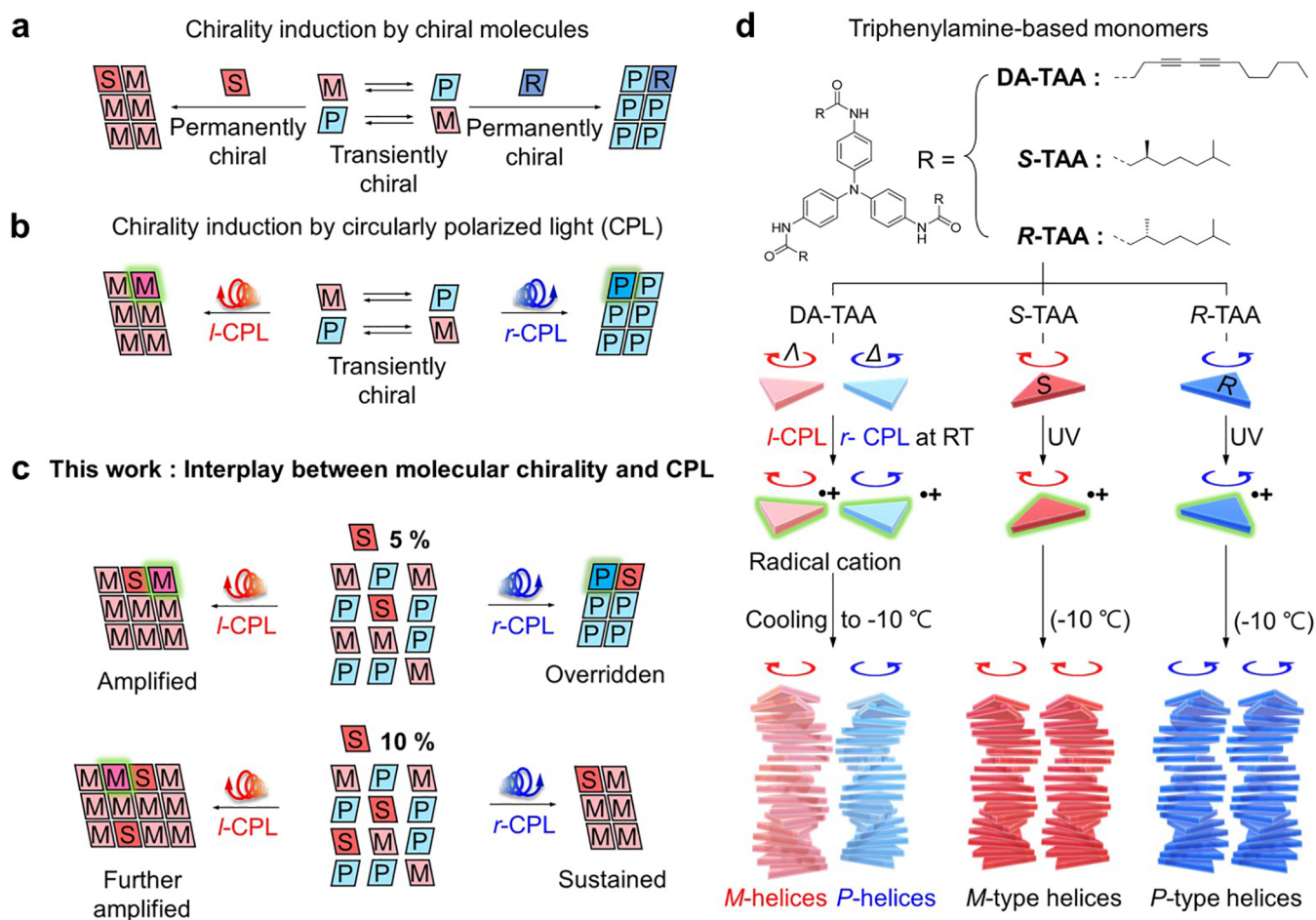


**Figure 1.** Transmission of chiral information from molecular chirality and CPL as an external input. (a) Chirality induction in transiently chiral molecules (soldiers) by a molecular chiral inducer (sergeant). (b) Chirality induction by CPL as a photonic sergeant. (c) Possible scenarios of chirality induction when molecular and photonic sergeants coexist. (d) System design for this study. DA-TAA was chosen as a transiently chiral molecule which responds to light to form radical cationic species and triggers supramolecular polymerization in solution. S- and R-TAA are molecular sergeants containing a stereocenter in the side chain. Their molecular configurations and resulting supramolecular helices, which formed upon light irradiation and subsequent cooling, are schematically depicted.

Although a mechanism has not been clearly proposed, this photon-to-matter chirality transfer is very comparable to chirality induction in the SaS process.

Here we reveal that CPL can act as a “photonic sergeant” by inducing symmetry breaking in the soldier molecule and competing with sergeant molecules in the chirality induction process. We first employed a supramolecular polymerization system, following the SaS process for CPL and a sergeant, and clarified the mechanism driving chirality control by CPL. Then we demonstrated four scenarios that can be realized depending on the amount of the sergeant molecule and the preferred handedness of both sergeants (Figure 1c). Matching the rotational direction of the CPL to the molecular configuration amplified supramolecular chirality cooperatively, while a mismatch offset the chiral response.

We further found that a critical amount of molecular sergeant exists that distinguishes regions of fixed and fluctuating supramolecular chirality. Above the threshold, the supramolecular chirality of the entire system persists, even upon exposure to CPL with the opposite direction. This result is consistent with the metastable nature of the prebiotic racemic state, which is stable against small fluctuations but eventually evolves into a homochiral state by accumulating

chiral bias above a critical e.e.<sup>2</sup> Overriding molecular chirality by light, and reverting supramolecular chirality, are both possible below the onset, and the “sergeant strength” of the CPL relative to the molecular sergeant can be quantified by using competitive experiments. This opens up new opportunities for the orthogonal control of supramolecular twisting direction, decoupled from molecular chirality preexisting in the system.

## RESULTS AND DISCUSSION

**System Design.** The supramolecular polymerizations we studied are based on triarylamine (TAA) molecules (Figure 1d; for synthetic details, see the Supporting Information and Figures S1–S3). With the  $C_3$  symmetry, the transiently chiral TAA motif can adopt  $\Delta$  (right-handed) and  $\Lambda$  (left-handed) conformations based on the twisted direction of the aromatic rings and stack into helices aided by 3-fold hydrogen bonds.<sup>27</sup> We chose tris(4-trideca-4,6-diynamidophenyl)amine (DA-TAA) as the soldier to utilize CPL as a photonic sergeant.<sup>25</sup> S- and R-TAA containing a chiral 3,7-dimethyloctyl side chain<sup>28</sup> were selected as molecular sergeants. We have previously reported that supramolecular helicity can be controlled by the rotational direction of incident CPL in the

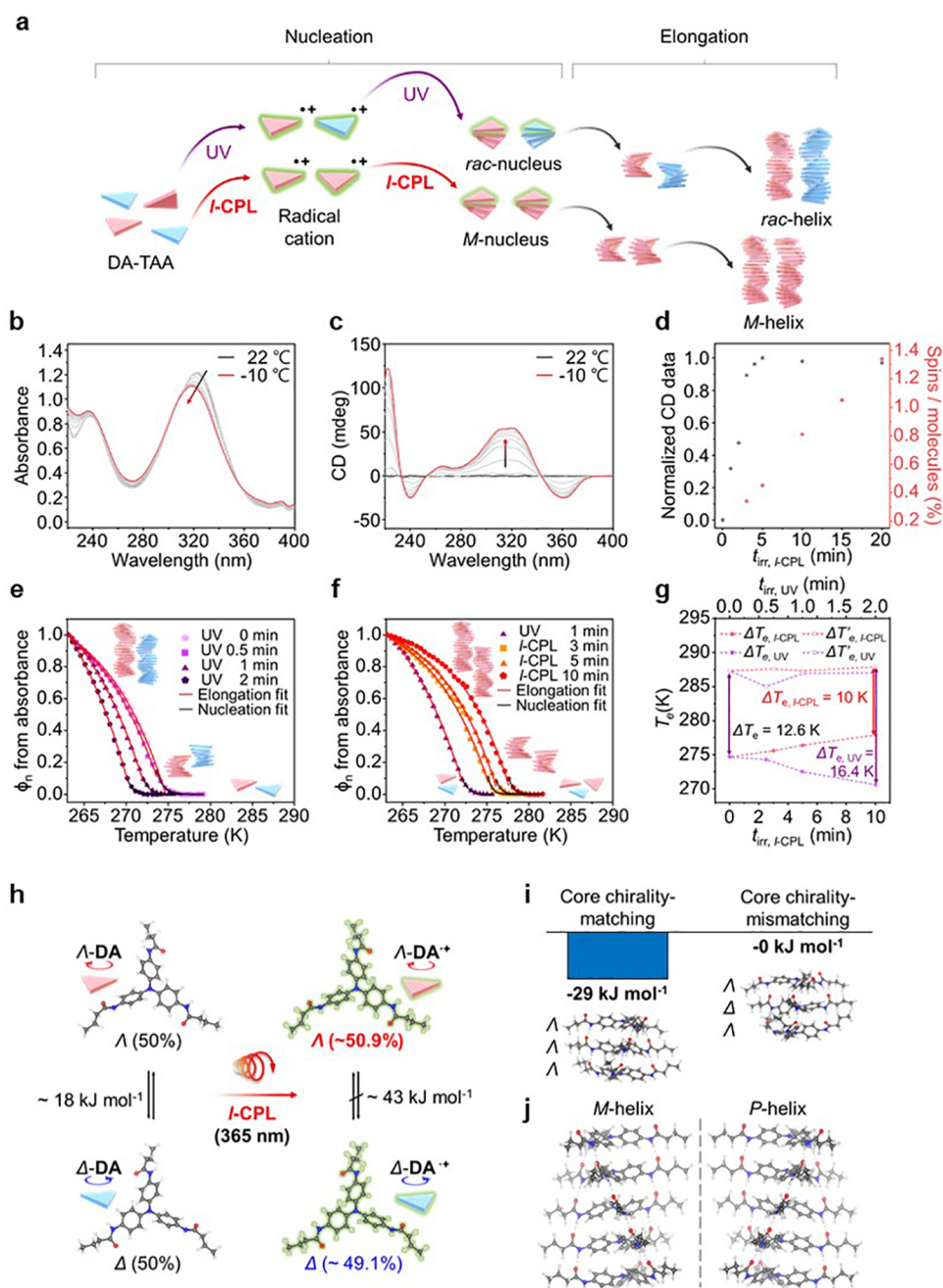


**Figure 2.** Supramolecular polymerization of DA-TAA upon light exposure. (a) Schematic depiction of the polymerization triggered by UV and *l*-CPL irradiation. (b) Temperature-dependent UV spectra upon UV irradiation for 1 min at room temperature followed by slow cooling to  $-10^{\circ}\text{C}$ . (c) Temperature-dependent CD spectra obtained with 5 min of *l*-CPL irradiation. (d) Evolution of CD intensity at 317 nm at  $-10^{\circ}\text{C}$  as a function of  $t_{\text{irr}, l\text{-CPL}}$ . The amount of radical species generated by *l*-CPL irradiation is also shown in the graph, which was quantified by EPR measurements at room temperature. (e, f) Growth of the polymerized fraction as a function of temperature during cooling. Each curve was fitted by using a cooperative model composed of nucleation (black line) and elongation (red line) steps. (e) UV irradiation with  $t_{\text{irr}}$  varied from 0 to 2 min. (f) *l*-CPL irradiation with  $t_{\text{irr}}$  from 3 to 10 min. (g) Elongation temperature  $T_e$  obtained from cooling and heating curves ( $T'_e$  and  $T_e$ ) as a function of  $t_{\text{irr}}$  for UV and *l*-CPL irradiation. (h) Computation of transition electric dipole strength for  $\Delta$ - and  $\Lambda$ -conformers upon *l*-CPL irradiation at 365 nm. Relative populations of each conformation in the neutral and radical cation states are shown, along with the computed rotational energy barriers. (i) DFT calculations for core chirality-matching and mismatching trimers (left:  $\Lambda$ - $\Lambda$ - $\Lambda$ ; right:  $\Lambda$ - $\Delta$ - $\Lambda$ ). Energy differences for the association of the DA-TAA radical cation with the neutral dimer are shown relative to  $\Lambda$ - $\Delta$ - $\Lambda$ . (j) DFT-calculated *M*- and *P*-helix structures.

photoinduced self-assembly of DA-TAA in chlorinated solvents, although the mechanism has remained elusive.<sup>25</sup> Supramolecular polymerization of TAA derivatives containing saturated alkyl side chains has been also studied by several groups.<sup>27,29–37</sup> The SaS principle was demonstrated for TAA-

containing compounds with sergeants possessing chiral side chains.<sup>37</sup>

**Evolution of Supramolecular Chirality by CPL.** Figure 2a schematically illustrates supramolecular polymerization of DA-TAA upon irradiation with unpolarized UV and CPL. A DA-TAA solution in 1,2-dichloroethane (DCE) was exposed



to light centered at 365 nm at room temperature for a designated time lapse ( $t_{\text{irr}}$ ). The supramolecular polymerization occurs upon slow cooling ( $-1\text{ }^{\circ}\text{C}/\text{min}$ ) as evidenced by a decrease of absorption intensity in the UV–vis spectra (Figure 2b and Figure S4). Together with a blue-shift of the absorption maximum from 322 to 317 nm, corresponding to  $\pi$ – $\pi^*$  transition, these changes show that the monomeric TAA units are polymerized via H-aggregation.<sup>28</sup> The UV and CPL irradiations produced virtually indistinguishable absorption spectral features.

In contrast, in the circular dichroism (CD) spectra, strong activity developed with a positive signal at 317 nm when the DA-TAA solution was exposed to *l*-CPL (Figure 2c).<sup>25</sup> No noticeable CD intensity was observed with the UV light source as expected. The enantioselective polymerization of DA-TAA by CPL is further supported by the mirror-imaged CD spectra produced with *r*-CPL and is consistent with our previous report (Figure S4c).<sup>25</sup> On the basis of the sign of the CD spectra, we determined that *l*- and *r*-CPL drove the preferential formation of left-handed *M*- and right-handed *P*-type helices, respectively. While the CD sign clearly indicates that a one-handed helical conformation proliferates over the other, we note it is not possible to quantify the helix composition in the CPL-irradiated solution because 100% single-handed-helix formation cannot be ensured. Gradual heating back to room temperature dissociated the assembly and eventually restored the molecularly dissolved DA-TAA. Complete dissociation occurs at a much higher temperature than the onset of polymerization during cooling, creating a hysteresis between cooling and heating.

When the normalized CD intensity at 317 nm at  $-10\text{ }^{\circ}\text{C}$  was plotted as a function of *l*-CPL irradiation time ( $t_{\text{irr},l\text{-CPL}}$ ), a rapid increase was observed followed by a plateau after 5 min (Figure 2d and Figure S4c,d). The strong positive and nonlinear deviation from a diagonal line is strikingly reminiscent of the CD intensity profiles found in SaS systems as a function of the molecular sergeant fraction, providing a compelling hint for interpreting CPL as a photonic sergeant.<sup>21</sup> Irradiation longer than 20 min decreased CD activity (Figure S4d). Within the NMR resolution limit, we did not observe noticeable degradation upon prolonged light exposure (Figure S5). It seems that generating a large number of radical cation species by light increases the positive charge density within the supramolecular aggregate, resulting in reduction in size by repelling the monomers inside.<sup>31,38</sup>

The normalized UV absorbance at 317 nm obtained upon UV and CPL irradiation with different  $t_{\text{irr}}$ s was converted into the polymerized fraction, assuming full conversion at  $-10\text{ }^{\circ}\text{C}$ , and plotted as a function of temperature in Figure 2e,f. The nonsigmoidal shape suggests the supramolecular polymerization follows a nucleation–elongation mechanism.<sup>39</sup> The cooperative model did indeed fit the data nicely, while the isodesmic fit failed (Figures S6–S8 and Tables S1–S3).<sup>28,39–41</sup> This suggests that the formation of a triarylammonium radical cation by light-induced oxidation could be responsible for nucleation since the radical cation–counteranion pairs as electric dipoles trigger stacking.<sup>29,31</sup> We confirmed formation of the radical species by electron paramagnetic resonance (EPR) spectroscopy for both UV and CPL irradiation (Figures S9 and S10). The decreased UV absorbance at 317 nm with the increasing absorption in the 700–800 nm range in UV–vis–NIR spectra also supports radical formation (Figure S11). While the slow cooling condition may not reflect true

thermodynamic control, the data obtained during slow heating back to room temperature could be also fitted by the cooperative model and showed similar trends to the cooling fits (Figure S7, Tables S1 and S2). Furthermore, the extracted enthalpy value for the elongation ( $\Delta H_e$ ) with UV irradiation was comparable to the  $\Delta H$  estimated by the van't Hoff plot in the same condition, supporting the reliability of the cooperative model (Figure S12 and Table S4). The CD intensity could also be fitted with the same model in the CPL case and gave qualitatively similar results (Figure S8 and Table S3).

Interestingly, the elongation temperature ( $T'_e$ ), which coincides with the onset temperature of polymerization, decreased with the increasing  $t_{\text{irr}}$  of UV irradiation, indicating a higher nucleation penalty. In contrast, longer CPL irradiation facilitated supramolecular polymerization, as evidenced by the increase in  $T'_e$ . The association constant  $K_a$  responsible for nucleation, and nucleation enthalpy  $\Delta H_n$  extracted from the fitting, were consistent with the accelerated and retarded nucleation observed upon CPL and UV exposure (Tables S1 and S2).

The disparity becomes more obvious by analyzing the hysteresis between the cooling and heating curves (Figure 2g). The  $T_e$  responsible for complete dissociation in the heating curve is primarily correlated to the intrinsic stability limit of the DA-TAA stacks and does not vary much with  $t_{\text{irr}}$  for both UV and CPL. The  $T_e$ – $T'_e$  gap ( $\Delta T_e$ ) in the hysteresis represents the metastable state in the nucleation stage where the monomers are kinetically inactive, unable to be polymerized.<sup>28,42,43</sup> Longer exposure to *l*-CPL narrows the gap by increasing  $T'_e$ , while the UV irradiation results in exactly the opposite behavior. The two trend lines meet at  $T'_e$  obtained without light exposure. In Figure 2g, the *l*-CPL and UV irradiation data were plotted together with a calibrated  $t_{\text{irr}}$  that induces similar conversion, as determined by UV absorbance. Quantification of the amount of the radical species by EPR spectroscopy supported that 5 min of *l*-CPL irradiation is comparable to 1 min of UV (Figure S10c).

Our data suggest that the intrinsic chirality in CPL is transmitted into the supramolecular polymer, probably via symmetry breaking in the nucleation stage, which involves the photoinduced formation of the DA-TAA radical cation. We employed density functional theory (DFT) calculations to investigate the photooxidation. Figure 2h depicts the ground-state  $\Lambda$  and  $\Delta$  conformations of neutral DA-TAA, separated by a rotational energy barrier of  $18\text{ kJ mol}^{-1}$  as a result of helical chirality (Table S5). The interconversion has been suggested to preferentially occur through a pathway where two phenyl groups rotate in one direction while the third one rotates in the opposite direction rather than concerted rotation in the same direction.<sup>44</sup> The flatter radical cation form also possesses the two conformations, even with a higher barrier ( $43\text{ kJ mol}^{-1}$ ). We postulate that photooxidation occurs at 365 nm radiation via excitation of an electron from the HOMO ( $\pi$ ) to the LUMO ( $\pi^*$ ), followed by charge transfer to the DCE solvent (Table S6). Time-dependent DFT computation suggests that the molar extinction coefficient of the  $\Lambda$  conformer to *l*-CPL should be 1.8% larger than  $\Delta$  at this wavelength (Table S7). This accounts for the photoresolution of the radical cation upon *l*-CPL exposure leading to enrichment of the  $\Lambda$ -form. Cross-transitions, such as  $\Delta$ -to- $\Lambda$ , are predicted to be negligible. Equal populations of  $\Delta$ - and  $\Lambda$ -species will be generated by UV irradiation.



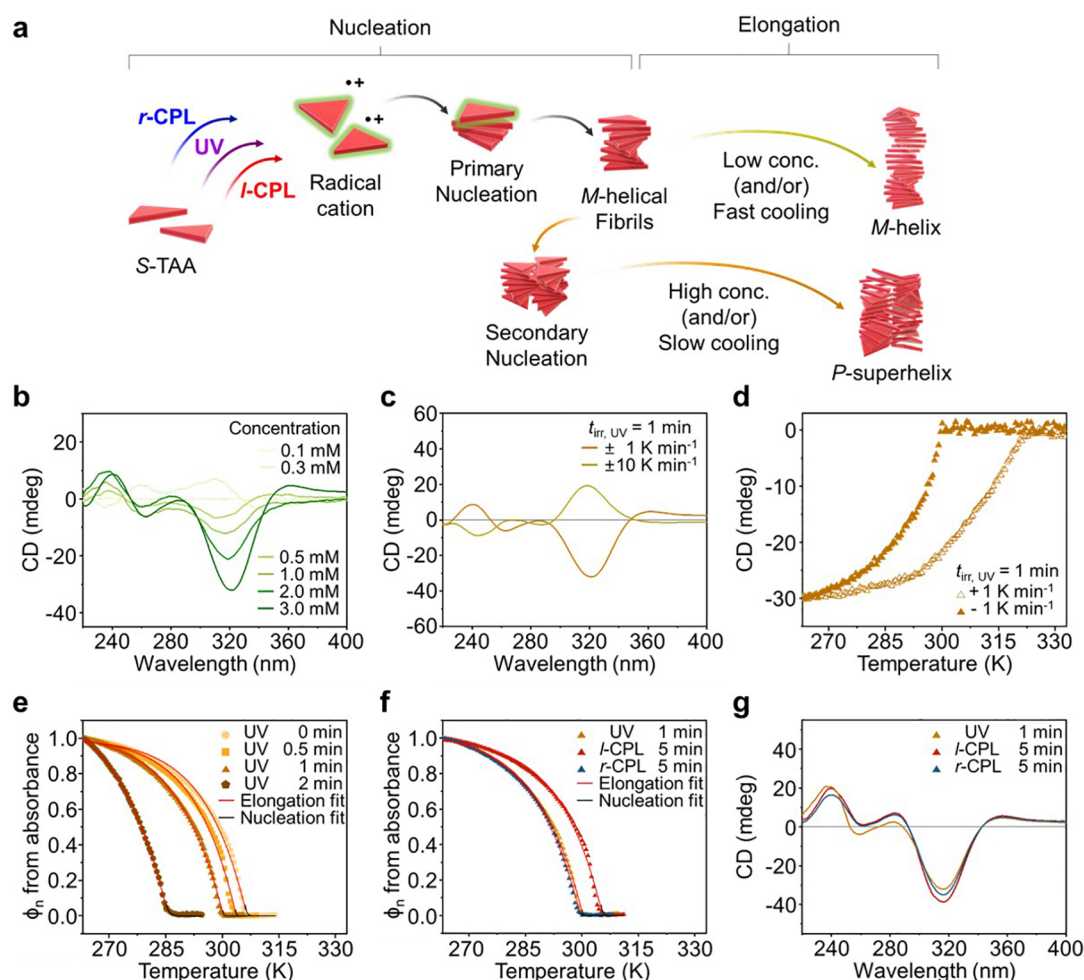


**Figure 3.** Supramolecular polymerization of S-TAA upon light exposure. (a) Schematic depiction of the polymerization depending on the concentration and the cooling rate. (b) CD spectra at various concentrations at  $-10\text{ }^{\circ}\text{C}$ . The data were obtained after UV irradiation for 1 min at  $80\text{ }^{\circ}\text{C}$  followed by slow cooling to  $-10\text{ }^{\circ}\text{C}$ . (c) CD spectra at  $-10\text{ }^{\circ}\text{C}$  obtained by slow and fast cooling ( $3.0\text{ mM}$ ,  $t_{\text{irr,UV}} = 1\text{ min}$ ). (d) Temperature-dependent CD intensity upon slow cooling ( $3.0\text{ mM}$ ,  $t_{\text{irr,UV}} = 1\text{ min}$ ). (e) Effect of  $t_{\text{irr,UV}}$  on growth of the polymerized fraction as a function of temperature during cooling. Each curve was fitted by a cooperative model composed of nucleation (black line) and elongation (red line) steps. (f, g) Effect of UV irradiation vs *l*- and *r*-CPL ( $3.0\text{ mM}$ , slow cooling). The irradiation time was adjusted to provide equivalent light flux based on the DA-TAA polymerization results. (f) UV-vis absorbance at  $317\text{ nm}$  as a function of temperature. (g) CD spectra at  $-10\text{ }^{\circ}\text{C}$ .

The radical cation mediates the nonlinear amplification of chiral information from CPL in the nucleation–elongation pathway by triggering the nucleation event. Aggregation of the radical cation–counteranion pairs as electric dipoles has been suggested to be primarily responsible for the formation of critical nuclei after accommodation of the counteranions in the periphery.<sup>32</sup> We note that the radical cations interact with themselves and also with the neutral TAA molecules as small clusters even at room temperature without nucleation, as evidenced by the disappearance of aromatic protons in  $^1\text{H}$  NMR spectra.<sup>26</sup> Although the rotational energy barrier itself is not large enough to prevent racemization of the radical cation at room temperature, such preferential aggregation involving the radical cations should effectively suppress racemization and keep the handedness induced by CPL (Table S8). From the EPR data, the number of the radical species gradually increased under longer exposure of both UV and CPL (Figure S13).<sup>32</sup> While this is expected to accelerate nucleation, delayed polymerization upon UV irradiation suggests that the radical species behave as retarders to the growing stack with the opposite conformation.<sup>45</sup> The enantiomeric cross-inhibition

will eventually form homochiral *P*- and *M*-nuclei with equal populations through the self-sorting process. This picture is consistent with the chirality synchronization scheme and accounts for conglomerate formation via enantiophobic interaction.<sup>11</sup> Increasing the e.e. of the radical cation with CPL activates the chirality induction route<sup>11</sup> and facilitates nucleation by the enantioselective formation of homochiral nuclei following the handedness of CPL.

DFT calculations supported that it is strongly favored to match the helical direction of the triple intermolecular hydrogen bonds in the oligomeric stacks (Figures S14 and S15, Tables S9 and S10). While the penalty for core configuration mismatch is relatively smaller, the accumulation of the error makes the assembly quite unstable compared to homochiral stacking (Figure 2i). This captures the origin of the enantiophobic interaction in the nucleation stage. We further estimated the relative magnitudes of the helical reversal penalty (HRP) and mismatch penalty (MMP) based on an extended SaS model (Figures S16 and S17, Table S11).<sup>46</sup> HRP was at least 1 order of magnitude larger than MMP, consistent with the literature,<sup>37,46–49</sup> suggesting there is a relatively small

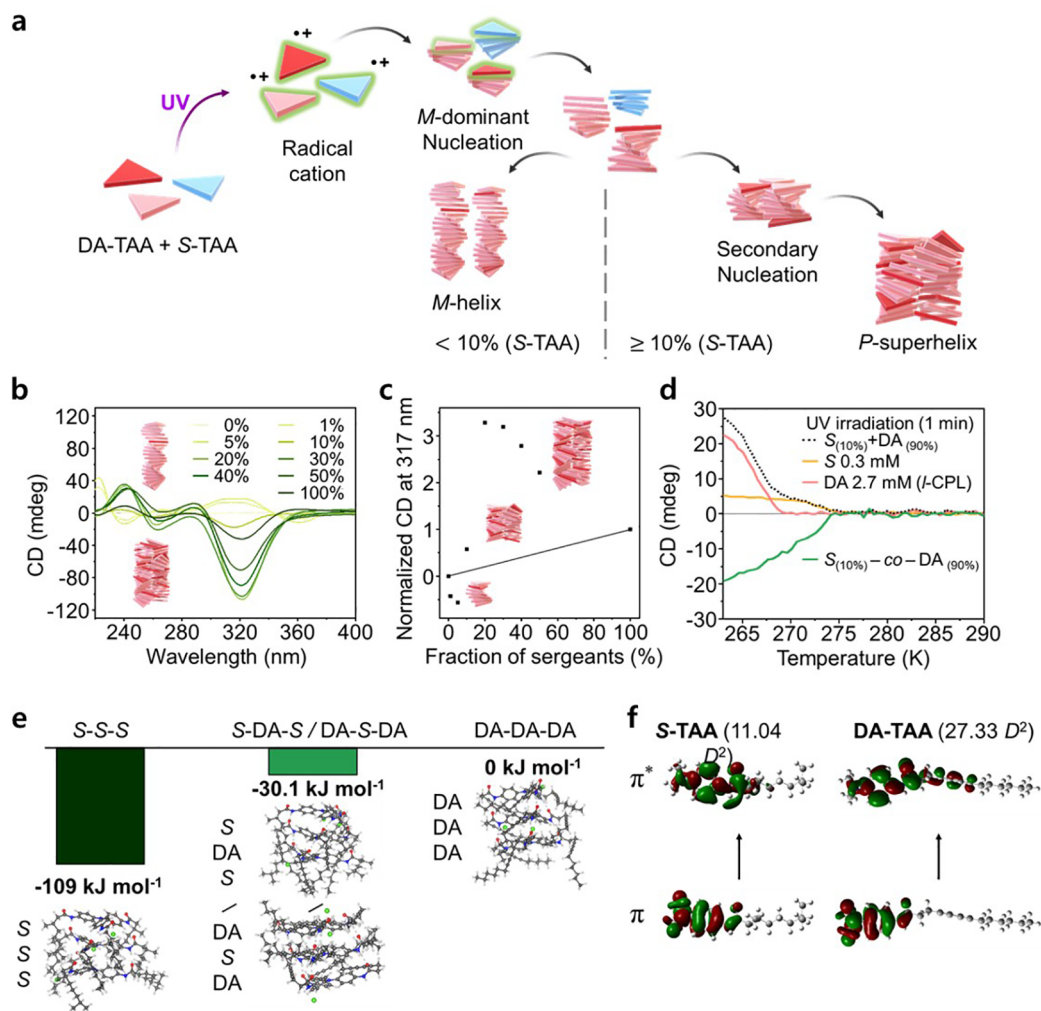


**Figure 4.** SaS coassembly of DA-TAA, with S-TAA as a molecular sergeant. (a) Schematic depiction of the copolymerization to M-helix and P-superhelix formation. (b) CD spectra at  $-10^{\circ}\text{C}$  with various S-TAA molar fractions. For the mixtures with a total concentration of 3.0 mM, the spectra were obtained after UV irradiation (1 min) followed by slow cooling. (c) CD intensity at 317 nm as a function of the S-TAA molar fraction. The intensity was normalized by 100% S-TAA. (d) Temperature-dependent CD intensity at 317 nm for the mixture containing 10% S-TAA (green solid line). Intensity profiles of 10% S-TAA alone (0.3 mM) under UV exposure (yellow solid line) and 90% DA-TAA (2.7 mM) upon *l*-CPL irradiation (pink solid line) are also shown for comparison, along with their linear sum (black dashed line). (e) DFT-calculated trimer stability for different combinations. Energy differences for the association of S-TAA and DA-TAA radical cation species to the trimer are exhibited relative to DA trimer. The energies of the trimer composed of S- and DA-TAA were averaged. (f) Computation of transition electric dipole strength for S- and DA-TAA for the  $\pi$ - $\pi^*$  transition. The highest value among the first three excitations is indicated.

energy penalty for incorporating a mismatched conformer as long as the handedness persists. The large HRP is probably related to the hydrogen bonds, which drive homohelical elongation with high fidelity and amplify the chiral information from CPL into the dominant helical sense (Figure 2j).<sup>46</sup>

**Molecular Sergeants.** Prior to the SaS experiments of DA-TAA with S- and R-TAA as molecular sergeants, we investigated the homoassembly behavior of S-TAA in DCE solution (Figure 3 and Figure S13). Upon slow cooling to  $-10^{\circ}\text{C}$ , an inversion appears in the CD sign at 317 nm, from positive to negative, as concentration increased above 0.3 mM (Figure 3b). This corresponds to a transition from M-helix to P-superhelix, which is formed by opposite coiling of the M-helices.<sup>28</sup> Atomic force microscopy imaging supported superhelix formation (Figure S18). Fast cooling ( $-10^{\circ}\text{C}/\text{min}$ ) also changed the CD sign as reported in the literature<sup>27</sup> (Figure 3c). No noticeable transition was found in the slow cooling curve monitored by CD and UV, revealing that P-superhelices

dominate almost instantaneously once the supramolecular polymerization is nucleated (Figure 3d and Figure S19).

We studied the effect of UV as a function of  $t_{\text{irr}}$  (Figure 3e, Figure S20, Tables S12 and S13). As in the case of DA-TAA, the temperature-dependent UV/CD intensities could be fitted by the cooperative model assuming a single nucleation step to M-helices or P-superhelices.<sup>28</sup> The much higher  $T'_e$  in the absence of irradiation indicates the strong propensity of S-TAA toward polymerization driven by packing of the stereoregular and less flexible side chain. Exposure to light retarded the supramolecular polymerization, marked by decreased  $T'_e$  and CD intensity. Because the nuclei formation now involves the radical cation and its core configuration cannot be enantiomerically pure even under the CPL irradiation, the contradicting core-periphery chirality in the radical population could be responsible for the retardation. Nonetheless, P-superhelices were consistently formed upon irradiation with *l*- and even *r*-CPL at the light flux equivalent to UV estimated by

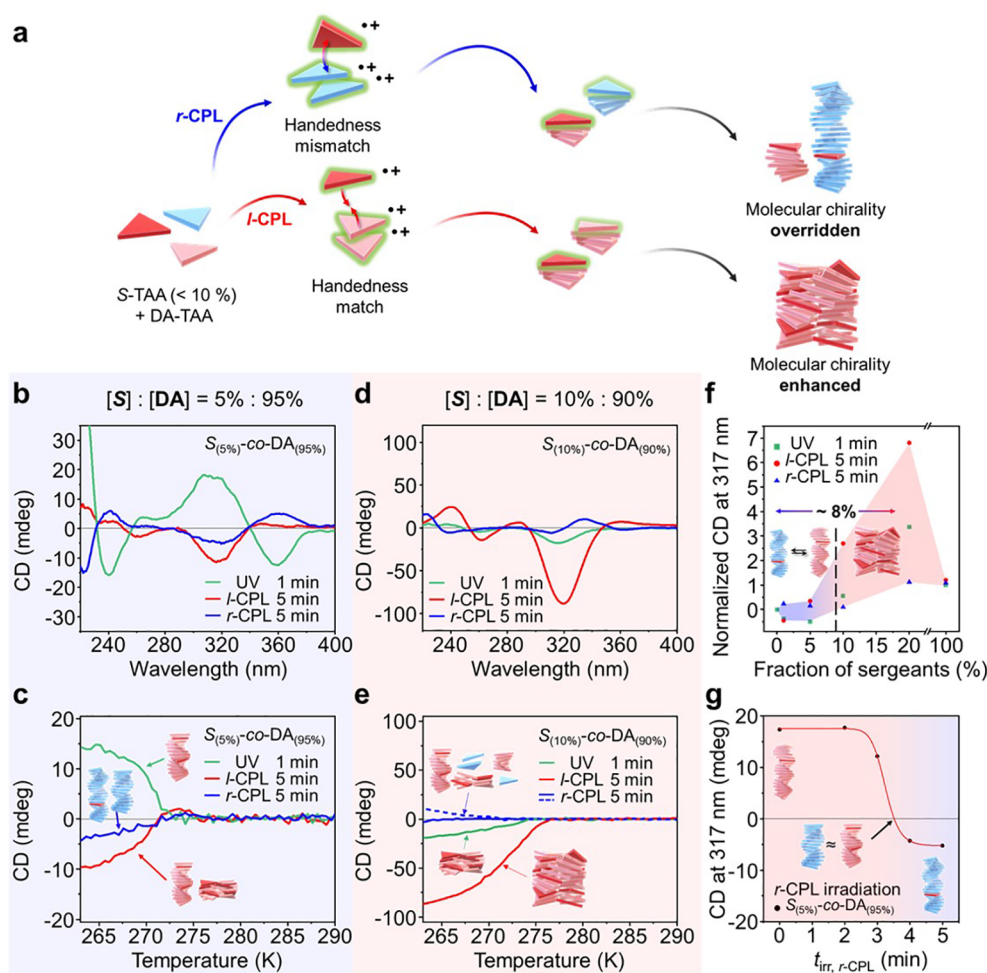


**Figure 5.** Amplifying and overriding molecular chiral information in the supramolecular state by CPL. (a) Schematic depiction of DA-TAA/S-TAA copolymerization upon *l*- and *r*-CPL exposure. (b–e) CD spectra at  $-10\text{ }^{\circ}\text{C}$  upon *l*-CPL (red), UV (green), and *r*-CPL (blue) exposure (b, d) and temperature-dependent CD intensity (c, e). (b, c) 5% S-TAA-containing mixture. (d, e) 10% S-TAA-containing mixture. For parts c and e, the peak intensity at 317 nm was plotted as a function of the sergeant fraction (blue dashed line). (f) Net helicity as a function of the S-TAA molar fraction. The net helicity was obtained as the CD intensity at 317 nm was normalized by 100% S-TAA. (g) Change in net helicity with increasing *r*-CPL irradiation time for the 5% S-TAA-containing mixture. A red line depicts a sigmoidal fit as a guide to the eye to show the crossover point.

the DA-TAA data (Figure 3f). Changes in the CD spectral features were negligible when the light source was switched to CPL (Figure 3g). The results confirm that the peripheral molecular chirality in S-TAA is primarily responsible for the twisting direction. We note that chirality matching the *l*-CPL exposure facilitates nucleation slightly, as evidenced by higher CD intensity,  $T'_e$ , and  $K_a$  than UV (Figure 3f, Figure S21, and Table S14).

Then we verified that DA-TAA can be copolymerized with S-TAA as a molecular sergeant (Figure 4). The SaS experiments were conducted by using mixtures of DA-TAA and S-TAA at a fixed total concentration (3.0 mM) under UV irradiation (Figure 4a). S-TAA effectively behaves as a  $\Lambda$ -sergeant, like *l*-CPL: *M*-helices were mainly produced below 10 mol % of S-TAA loading, and *P*-superhelices populated above (Figure 4b). The helix–superhelix transition generates a negative extremum at 5% when the CD intensity, normalized to 100% S-TAA, is plotted as a function of the sergeant fraction (Figure 4c). Unlike the typical trend observed in SaS systems,<sup>22</sup> a positive extremum also appears at 20% S-TAA. The CD intensity then decreases monotonically above the

fraction to 100%. The CD intensity, correlated to the net helicity, was anomalously amplified more than 3-fold at 20% S-TAA compared to the pure sergeant. We consider that contribution of orientation artifacts to the CD spectra is not significant based on the weak linear dichroism intensities (Figure S22).<sup>50</sup>

Consistent with the coassembly behavior, a single  $T'_e$  was identified in the temperature-dependent CD measurement at 10% S-TAA, which produced *P*-superhelices upon cooling (Figure 4d). The possibility of S- and DA-TAA homopolymerizations can be ruled out by comparing the cooling curve to the individual S-TAA (0.3 mM) and DA-TAA (2.7 mM) data showing *M*-helix formation (Figures S23–S27).<sup>35</sup> The  $T'_e$  of the copolymerization was very close to that of S-TAA alone, but notably higher than DA-TAA, suggesting that S-TAA is strongly involved in the nucleation step despite its low population.<sup>35</sup> The EPR data indicated that S-TAA produced radical species nearly 3 times more than DA-TAA in the single solution and also in the mixture, supporting the strong contribution of S-TAA in nucleation (Figures S28 and S29). We also observed that more than 50% of the radical species



persists at  $-10\text{ }^{\circ}\text{C}$  and below (Figure S30). The change in the hyperfine splitting patterns upon cooling suggests that the unpaired electrons localized on one TAA at room temperature become more delocalized between TAA molecules.<sup>38</sup> DFT calculations also supported the preferential association of S-TAA (Figure 4e and Table S15). The transition dipole moment calculation for the  $\pi-\pi^*$  transition further revealed that the rotatory strength of the DA-TAA is more than 2 times larger than S-TAA because of the contribution of the diacetylene moiety in the side chain (Figure 4f and Table S16). The high rotatory strength originating from the diacetylene-containing side chain is also responsible for strong CD intensity.<sup>51</sup> The coassembly of strong helicity-driving sergeants with optically more active soldiers results in anomalous chiral amplification in CD intensity.

**Amplification and Overriding of Supramolecular Chirality by CPL.** We performed SaS experiments for the DA-TAA/S-TAA mixtures upon exposure to CPL (Figure 5). At 5% S-TAA loading, in contrast to UV irradiation, it was evident that the CPL handedness determines the screw sense of the supramolecular polymer. While the UV-primed coassembly formed *M*-helices driven by S-TAA with a positive CD sign at 317 nm, both *l*- and *r*-CPL irradiation produced negative CD activity with different intensities (Figure 5b).

On the basis of the spectral features at 360 nm and below 240 nm, we identified *P*-helix and *P*-superhelix as the major species generated by the *r*- and *l*-CPL, respectively. A positive CD maximum at 360 nm with strong negative CD intensity below 240 nm was observed upon *r*-CPL exposure. These features are consistent with the CD spectra of DA-TAA irradiated with *r*-CPL (Figure S4c), indicating that *r*-CPL overrode the chiral information from S-TAA and generated *P*-helices. In contrast, an extremum was not observed at 360 nm when *l*-CPL was irradiated, and the CD intensity below 240 nm was much weaker. This corresponds to the formation of *P*-superhelices (Figure 4b), supporting amplification of chiral response by handedness-matching *l*-CPL. Because a transition from the *M*-helix to *P*-superhelix was observed above 8% S-TAA loading under UV irradiation, the amplified response by *l*-CPL was attributed to be comparable to the 3% increased S-TAA fraction (Figure S31). At this molecular sergeant content, nucleus chirality seems to be dominated by DA-TAA radical cations, partially photoresolved by CPL. Interestingly, retardation in  $T'_e$  by UV irradiation was not found in the temperature-dependent CD measurements, probably because of the activated nucleation in the presence of S-TAA (Figure 5c and Figures S32–S34).

Increasing the S-TAA concentration accumulates chiral bias in the system to a point where helicity cannot be reverted by CPL anymore. In our system, the bifurcation point seemed to be  $\sim 8\%$  S-TAA: irradiating the mixture with *r*-CPL nearly canceled CD activity but left faint negative and positive intensities around 317 and 330 nm (Figure 5d and Figure S31b). The spectral shape combines features of the DA-TAA under *l*-CPL irradiation (forming *M*-helix) and the 10% S-TAA/90% DA-TAA under UV (forming *P*-superhelix). A qualitatively similar spectrum could be reproduced by a linear sum of the individual CD spectra (Figure S35). While the *P*-superhelix population is suppressed by interference with *r*-CPL, the left-handedness set by the S-TAA persists and cannot be overridden by the CPL. As expected, chirality-matching the *l*-CPL boosts the CD response by more than 4 times compared to UV irradiation.  $T'_e$  values were also in order of *l*-CPL > UV

> *r*-CPL, consistent with the constructive and destructive interactions between the molecular chirality and the external chirality encoded in light (Figure 5e, Figures S36 and S37). Using R-TAA as the sergeant gave exactly mirror-imaged results (Figure S38). We further increased the S-TAA content to 20% and observed identical behavior. Relative to the CD intensity obtained with 20% S-TAA alone, the net helicity was amplified by nearly 700% in the SaS system by the synergistic contributions of the photonic and molecular sergeants (Figure 5f and Figure S39).

Finally, we attempted to quantify the sergeant strength of the CPL as a function of  $t_{\text{irr}}$  relative to S-TAA content. The 5% S-TAA mixture was selected because it was possible to override the molecular chiral information with *r*-CPL (Figure 5g and Figure S40). Up to 3 min of irradiation, the net helicity followed the handedness provided by the S-TAA. We posit that in this regime nucleation is driven by the S-TAA, as the amount of radical cation species generated by irradiation is not sufficient. A gradual transition between 3 and 4 min resulted in helicity inversion, from *M*-helix to the opposite *P*-form. On the basis of the light intensity, we estimate that  $2.5 \times 10^6$  *r*-CPL photons are roughly equivalent to 1 S-TAA molecule. Based on the EPR data and the DFT calculation, estimating the amount of enantiomeric DA-TAA radical cations generated under 4 min of *r*-CPL exposure suggests that more than one enantiomeric radical out of 15000 molecules (including 750 sergeants) seems necessary for induction of the major helicity of the supramolecular polymer by CPL. Further irradiating with *r*-CPL up to 10 min produced strong CD intensity comparable to pure DA-TAA (Figure S4c), supporting that the chiral information from the molecular sergeant can be overridden in the supramolecular level by light.

## CONCLUSION

We have shown that supramolecular chirality can emerge from a transiently chiral molecular building block by transmitting chiral information inherited from the CPL. The light-induced supramolecular polymerization occurs via a nucleation–elongation pathway, which is triggered by the photoinduced formation of radical cations and followed by helical stacking. Photoresolution breaks the symmetry in the left- and right-handed radical conformers and accelerates the formation of nuclei with a specific screw sense that coincides with the CPL handedness via enantiophobic interaction. The nonlinear amplification of helicity as a function of CPL irradiation time is strongly reminiscent of the chirality induction expressed by the sergeants-and-soldier principle, which is found in the coassembly of a transiently chiral soldier with a permanently chiral sergeant.

Sergeants-and-soldier experiments with CPL irradiation showed that the conformational core chirality of the radical induced by the CPL competes with the chiral information about the stereocenter in the sergeant side chain. Matching the handedness of the CPL to the sergeant direction produced an anomalously amplified chiral response. For the CPL with mismatched handedness, a critical molar fraction of the sergeant was found for bifurcation: above a threshold, the helicity determined by the sergeant persisted. A fluctuation regime appeared below the fraction, where the CPL can override the molecular chirality with increasing irradiation time.

While the role of deterministic chiral stimuli such as CPL in the evolution of homochirality is controversial,<sup>2,18</sup> our results

suggest that the critical chiral bias can be accumulated during the chirality induction process, allowing the system to evolve into the homochiral state against racemization and also random external stimuli. Our results also demonstrate that supramolecular chirality can be developed following the handedness of the external stimuli and overturning the one imposed by molecular constraints, at least to some extent, which will open up new opportunities for designing multiscale chiral systems.

## ■ ASSOCIATED CONTENT

### Supporting Information

The Supporting Information is available free of charge at <https://pubs.acs.org/doi/10.1021/jacs.1c11306>.

Synthetic procedures, characterization and irradiation protocol of TAA derivatives, UV, CD, LD, and EPR spectroscopies, AFM imaging, details of modeling procedures of thermodynamic model, SaS model, and supporting figures and tables (PDF)

## ■ AUTHOR INFORMATION

### Corresponding Author

Myungeun Seo – Department of Chemistry, Korea Advanced Institute of Science and Technology (KAIST), Daejeon 34141, Korea; KAIST Institute for the Nanocentury, KAIST, Daejeon 34141, Korea; [orcid.org/0000-0002-5218-3502](https://orcid.org/0000-0002-5218-3502); Email: [seomyungeun@kaist.ac.kr](mailto:seomyungeun@kaist.ac.kr)

### Authors

Jun Su Kang – Department of Chemistry, Korea Advanced Institute of Science and Technology (KAIST), Daejeon 34141, Korea; [orcid.org/0000-0003-1417-3482](https://orcid.org/0000-0003-1417-3482)  
Sungwoo Kang – Department of Chemistry, Korea Advanced Institute of Science and Technology (KAIST), Daejeon 34141, Korea; [orcid.org/0000-0002-8830-5030](https://orcid.org/0000-0002-8830-5030)  
Jong-Min Suh – Department of Chemistry, Korea Advanced Institute of Science and Technology (KAIST), Daejeon 34141, Korea  
Soon Mo Park – Graduate School of Nanoscience and Technology, Korea Advanced Institute of Science and Technology (KAIST), Daejeon 34141, Korea  
Dong Ki Yoon – Department of Chemistry and Graduate School of Nanoscience and Technology, Korea Advanced Institute of Science and Technology (KAIST), Daejeon 34141, Korea; KAIST Institute for the Nanocentury, KAIST, Daejeon 34141, Korea; [orcid.org/0000-0002-9383-8958](https://orcid.org/0000-0002-9383-8958)  
Mi Hee Lim – Department of Chemistry, Korea Advanced Institute of Science and Technology (KAIST), Daejeon 34141, Korea; [orcid.org/0000-0003-3377-4996](https://orcid.org/0000-0003-3377-4996)  
Woo Youn Kim – Department of Chemistry, Korea Advanced Institute of Science and Technology (KAIST), Daejeon 34141, Korea; [orcid.org/0000-0001-7152-2111](https://orcid.org/0000-0001-7152-2111)

Complete contact information is available at:

<https://pubs.acs.org/doi/10.1021/jacs.1c11306>

### Notes

The authors declare no competing financial interest.

## ■ ACKNOWLEDGMENTS

This research was supported by the National Research Foundation of Korea (NRF) Grant funded by the Korean government (MSIT; No. 2018R1A5A1025208). M.H.L.

acknowledges NRF-2016R1A5A1009405 for financial support. The EPR experiment was supported by the Institute for Basic Science (IBS-R010-D1) in Korea.

## ■ REFERENCES

- (1) Blackmond, D. G. The Origin of Biological Homochirality. *Cold Spring Harbor Perspect. Biol.* **2010**, *2*, a002147.
- (2) Mason, S. F. Origins of biomolecular handedness. *Nature* **1984**, *311* (1984), 19–23.
- (3) Bailey, J.; Chrysostomou, A.; Hough, J. H.; Gledhill, T. M.; McCall, A.; Clark, S.; Ménard, F.; Tamura, M. Circular Polarization in Star-Formation Regions: Implications for Biomolecular Homochirality. *Science* **1998**, *281*, 672–674.
- (4) Modica, P.; Meinert, C.; de Marcellus, P.; Nahon, L.; Meierhenrich, U. J.; d'Hendecourt, L. L. S. Enantiomeric excesses induced in amino acids by ultraviolet circularly polarized light irradiation of extraterrestrial ice analogs: A possible source of asymmetry for prebiotic chemistry. *Astrophys. J.* **2014**, *788*, 79–89.
- (5) Feringa, B. L.; Van Delden, R. A. Absolute asymmetric synthesis: the origin, control, and amplification of chirality. *Angew. Chem., Int. Ed.* **1999**, *38*, 3418–3438.
- (6) Inoue, Y. Asymmetric photochemical reactions in solution. *Chem. Rev.* **1992**, *92*, 741–770.
- (7) Flores, J. J.; Bonner, W. A.; Massey, G. A. Asymmetric photolysis of (RS)-leucine with circularly polarized ultraviolet light. *J. Am. Chem. Soc.* **1977**, *99*, 3622–3625.
- (8) Meinert, C.; Filippi, J.-J.; Nahon, L.; Hoffmann, S. V.; D'Henecourt, L.; De Marcellus, P.; Brehéfort, J. H.; Thiemann, W. H.-P.; Meierhenrich, U. J. Photochirogenesis: photochemical models on the origin of biomolecular homochirality. *Symmetry* **2010**, *2*, 1055–1080.
- (9) Kawasaki, T.; Sato, M.; Ishiguro, S.; Saito, T.; Morishita, Y.; Sato, I.; Nishino, H.; Inoue, Y.; Soai, K. Enantioselective synthesis of near enantiopure compound by asymmetric autocatalysis triggered by asymmetric photolysis with circularly polarized light. *J. Am. Chem. Soc.* **2005**, *127*, 3274–3275.
- (10) Noorduyn, W. L.; Bode, A. A. C.; van der Meijden, M.; Meekes, H.; van Etteger, A. F.; van Enckevort, W. J. P.; Christianen, P. C. M.; Kaptein, B.; Kellogg, R. M.; Rasing, T.; Vlieg, E. Complete chiral symmetry breaking of an amino acid derivative directed by circularly polarized light. *Nat. Chem.* **2009**, *1*, 729–732.
- (11) Tschierske, C.; Ungar, G. Mirror symmetry breaking by chirality synchronisation in liquids and liquid crystals of achiral molecules. *ChemPhysChem* **2016**, *17*, 9–26.
- (12) Burnham, K. S.; Schuster, G. B. Transfer of chirality from circularly polarized light to a bulk material property: propagation of photoresolution by a liquid crystal transition. *J. Am. Chem. Soc.* **1999**, *121*, 10245–10246.
- (13) Huck, N. P. M.; Jager, W. F.; de Lange, B.; Feringa, B. L. Dynamic control and amplification of molecular chirality by circular polarized light. *Science* **1996**, *273*, 1686–1688.
- (14) Choi, S.-W.; Izumi, T.; Hoshino, Y.; Takanishi, Y.; Ishikawa, K.; Watanabe, J.; Takezoe, H. Circular-polarization-induced enantiomeric excess in liquid crystals of an achiral, bent-shaped mesogen. *Angew. Chem. Int.* **2006**, *118*, 1410–1413.
- (15) Tejedor, R. M.; Oriol, L.; Serrano, J. L.; Urena, F. P.; Gonzalez, J. J. L. Photoinduced chiral nematic organization in an achiral glassy nematic azopolymer. *Adv. Funct. Mater.* **2007**, *17*, 3486–3492.
- (16) Li, J.; Schuster, G. B.; Cheon, K.-S.; Green, M. M.; Selinger, J. V. Switching a helical polymer between mirror images using circularly polarized light. *J. Am. Chem. Soc.* **2000**, *122*, 2603–2612.
- (17) Wang, Y.; Harada, T.; Phuong, L. Q.; Kanemitsu, Y.; Nakano, T. Helix Induction to Polyfluorenes Using Circularly Polarized Light: Chirality Amplification, Phase-Selective Induction, and Anisotropic Emission. *Macromolecules* **2018**, *51*, 6865–6877.
- (18) Vandenbussche, S.; Reisse, J.; Bartik, K.; Lievin, J. The search for a deterministic origin for the presence of nonracemic amino-acids

in meteorites: a computational approach. *Chirality* **2011**, *23*, 367–373.

(19) Kulkarni, C.; Curvers, R. H. N.; Vantomme, G.; Broer, D.; Palmans, A. R. A.; Meskers, S. C. J.; Meijer, E. W. Consequences of Chirality in Directing the Pathway of Cholesteric Helix Inversion of  $\pi$ -Conjugated Polymers by Light. *Adv. Mater.* **2021**, *33*, 2005720.

(20) Liu, M.; Zhang, L.; Wang, T. Supramolecular chirality in self-assembled systems. *Chem. Rev.* **2015**, *115*, 7304–7397.

(21) Morrow, S. M.; Bissette, A. J.; Fletcher, S. P. Transmission of chirality through space and across length scales. *Nat. Nanotechnol.* **2017**, *12*, 410–419.

(22) Palmans, A. R. A.; Meijer, E. W. Amplification of chirality in dynamic supramolecular aggregates. *Angew. Chem., Int. Ed.* **2007**, *46*, 8948–8968.

(23) Hu, J.; Zhu, T.; He, C.; Zhang, Y.; Zhang, Q.; Zou, G. Chiral induction, transfer and modulation in  $C_3$ -symmetric columnar liquid crystalline assemblies. *J. Mater. Chem. C* **2017**, *5*, 5135–5142.

(24) Hu, J.; Xie, Y.; Zhang, H.; He, C.; Zhang, Q.; Zou, G. Chiral induction, modulation and locking in porphyrin based supramolecular assemblies with circularly polarized light. *Chem. Commun.* **2019**, *55*, 4953–4956.

(25) Kim, J.; Lee, J.; Kim, W. Y.; Kim, H.; Lee, S.; Lee, H. C.; Lee, Y. S.; Seo, M.; Kim, S. Y. Induction and control of supramolecular chirality by light in self-assembled helical nanostructures. *Nat. Commun.* **2015**, *6*, 6959–6966.

(26) Park, C.; Lee, J.; Kim, T.; Lim, J.; Park, J.; Kim, W. Y.; Kim, S. Y. Homochiral Supramolecular Thin Film from Self-Assembly of Achiral Triarylamine Molecules by Circularly Polarized Light. *Molecules* **2020**, *25*, 402–414.

(27) Moulin, E.; Armao, J. J., IV; Giuseppone, N. Triarylamine-based supramolecular polymers: structures, dynamics, and functions. *Acc. Chem. Res.* **2019**, *52*, 975–983.

(28) Osypenko, A.; Moulin, E.; Gavat, O.; Fuks, G.; Maaloum, M.; Koenis, M.; Buma, W. J.; Giuseppone, N. Temperature Control of Sequential Nucleation-Growth Mechanisms in Hierarchical Supramolecular Polymers. *Chem.—Eur. J.* **2019**, *25*, 13008–13016.

(29) Moulin, E.; Niess, F.; Maaloum, M.; Buhler, E.; Nyrkova, I.; Giuseppone, N. The hierarchical self-assembly of charge nanocarriers: a highly cooperative process promoted by visible light. *Angew. Chem., Int. Ed.* **2010**, *49*, 6974–6978.

(30) Faramarzi, V.; Niess, F.; Moulin, E.; Maaloum, M.; Dayen, J.-F.; Beaufrand, J.-B.; Zanettini, S.; Doudin, B.; Giuseppone, N. Light-triggered self-construction of supramolecular organic nanowires as metallic interconnects. *Nat. Chem.* **2012**, *4*, 485–490.

(31) Nyrkova, I.; Moulin, E.; Armao, J. J.; Maaloum, M.; Heinrich, B.; Rawiso, M.; Niess, F.; Cid, J.-J.; Jouault, N.; Buhler, E.; Semenov, A. N.; Giuseppone, N. Supramolecular self-assembly and radical kinetics in conducting self-replicating nanowires. *ACS Nano* **2014**, *8*, 10111–10124.

(32) Armao, J. J.; Nyrkova, I.; Fuks, G.; Osypenko, A.; Maaloum, M.; Moulin, E.; Arenal, R.; Gavat, O.; Semenov, A.; Giuseppone, N. Anisotropic self-assembly of supramolecular polymers and plasmonic nanoparticles at the liquid-liquid interface. *J. Am. Chem. Soc.* **2017**, *139*, 2345–2350.

(33) Koenis, M. A.; Osypenko, A.; Fuks, G.; Giuseppone, N.; Nicu, V. P.; Visscher, L.; Buma, W. J. Self-assembly of supramolecular polymers of N-centered triarylamine trisamides in the light of circular dichroism: reaching consensus between electrons and nuclei. *J. Am. Chem. Soc.* **2020**, *142*, 1020–1028.

(34) Adelizzi, B.; Filot, I. A. W.; Palmans, A. R. A.; Meijer, E. W. Unravelling the Pathway Complexity in Conformationally Flexible N-Centered Triarylamine Trisamides. *Chem.—Eur. J.* **2017**, *23*, 6103–6110.

(35) Adelizzi, B.; Aloï, A.; Markvoort, A. J.; Ten Eikelder, H. M. M.; Voets, I. K.; Palmans, A. R. A.; Meijer, E. W. Supramolecular block copolymers under thermodynamic control. *J. Am. Chem. Soc.* **2018**, *140*, 7168–7175.

(36) Seo, H.; Go, M.; Choi, H.; Kim, K. Y.; Choi, Y.; Lee, S. S.; Jung, S. H.; Jung, J. H. Peculiar Triarylamine-Based Co-assembled

Supramolecular Polymers That Exhibit Two Transition Temperatures in the Formation of a Coiled Helical Bundle. *Chem.—Asian J.* **2018**, *13*, 2847–2853.

(37) Kim, T.; Mori, T.; Aida, T.; Miyajima, D. Dynamic propeller conformation for the unprecedentedly high degree of chiral amplification of supramolecular helices. *Chem. Sci.* **2016**, *7*, 6689–6694.

(38) Armao, J. J.; Maaloum, M.; Ellis, T.; Fuks, G.; Rawiso, M.; Moulin, E.; Giuseppone, N. Healable Supramolecular Polymers as Organic Metals. *J. Am. Chem. Soc.* **2014**, *136*, 11382–11388.

(39) Smulders, M. M. J.; Schenning, A. P. H. J.; Meijer, E. W. Insight into the mechanisms of cooperative self-assembly: the “sergeants-and-soldiers” principle of chiral and achiral  $C_3$ -symmetry discotic triamides. *J. Am. Chem. Soc.* **2008**, *130*, 606–611.

(40) Smulders, M. M. J.; Niruwenhuisen, M. M. L.; De Greef, T. E. A.; Van der Schoot, P.; Schenning, A. P. H. J.; Meijer, E. W. How to distinguish isodesmic from cooperative supramolecular polymerization. *Chem.—Eur. J.* **2010**, *16*, 362–367.

(41) De Greef, T. F. A.; Smulders, M. M. J.; Wolffs, M.; Schenning, A. P. H. J.; Sijbesma, R. P.; Meijer, E. W. Supramolecular polymerization. *Chem. Rev.* **2009**, *109*, 5687–5754.

(42) Schulman, B.; Winfree, E. Synthesis of crystals with a programmable kinetic barrier to nucleation. *Proc. Natl. Acad. Sci. U. S. A.* **2007**, *104*, 15236–15241.

(43) Reva, I.; Lapinski, L.; Chattopadhyay, N.; Fausto, R. Vibrational spectrum and molecular structure of triphenylamine monomer: A combined matrix-isolation FTIR and theoretical study. *Phys. Chem. Chem. Phys.* **2003**, *5*, 3844–3850.

(44) Ogi, S.; Stepanenko, V.; Sugiyasu, K.; Takeuchi, M.; Würthner, F. Mechanism of self-assembly process and seeded supramolecular polymerization of perylene bisimide organogelator. *J. Am. Chem. Soc.* **2015**, *137*, 3300–3307.

(45) Sandars, P. G. H. A toy model for the generation of homochirality during polymerization. *Origins of Life and Evol. Biosphere* **2003**, *33*, 575–587.

(46) Smulders, M. M. J.; Filot, I. A. W.; Leenders, J. M. A.; Van der Schoot, P.; Palmans, A. R. A.; Schenning, A. P. H. J.; Meijer, E. W. Tuning the extent of chiral amplification by temperature in a dynamic supramolecular polymer. *J. Am. Chem. Soc.* **2010**, *132*, 611–619.

(47) Van Gestel, J.; Palmans, A. R. A.; Titulaer, B.; Vekemans, J. A. J. M.; Meijer, E. W. “Majority-Rules” Operative in Chiral Columnar Stacks of  $C_3$ -Symmetrical Molecules. *J. Am. Chem. Soc.* **2005**, *127*, 5490–5494.

(48) Greciano, E. E.; Calbo, J.; Buendía, J.; Cerdá, J.; Aragón, J.; Orti, E.; Sánchez, L. Decoding the consequences of increasing the size of self-assembling tricarboxamides on chiral amplification. *J. Am. Chem. Soc.* **2019**, *141*, 7463–7472.

(49) Shindo, Y.; Nishio, M. The effect of linear anisotropies on the CD spectrum: Is it true that the oriented polyvinylalcohol film has a magic chiral domain inducing optical activity in achiral molecules? *Biopolymers* **1990**, *30*, 25–31.

(50) Helmich, F.; Smulders, M. M. J.; Lee, C. C.; Schenning, A. P. H. J.; Meijer, E. W. Effect of Stereogenic Centers on the Self-Sorting, Depolymerization, and Atropisomerization Kinetics of Porphyrin-Based Aggregates. *Angew. Chem., Int. Ed.* **2011**, *133*, 12238–12246.

(51) Didraga, C.; Klugkist, J. A.; Knoester, J. Optical properties of helical cylindrical molecular aggregates: the homogeneous limit. *J. Phys. Chem. B* **2002**, *106*, 11474–11486.